HEDL-SA 2006 FP

CONF-800607--88

FAILURE ANALYSIS OF CARBIDE FUELS UNDER TRANSIENT OVERPOWER (TOP) CONDITIONS

D. H. Nguyen

June 1980

American Nuclear Society

June 9-11, 1980

Las Vegas, Nevada

HANFORD ENGINEERING DEVELOPMENT LABORATORY
Operated by Westinghouse Hanford Company, a subsidiary of Westinghouse Electric Corporation, under the Department of Energy Contract No. DE-AC14-76FF02170

DISCLAIMER

CONTENTS

	Page
Abstract	iii
Figures	vi
Tables	vii
I. Introduction	1
II. Carbide Fuel Preconditioning Calculations	2
III. Determination of Fuel Failure	15
IV. Summary and Conclusions	35
V. References	40

THIS PAGE

WAS INTENTIONALLY

LEFT BLANK

FAILURE ANALYSIS OF CARBIDE FUELS UNDER TRANSIENT OVERPOWER (TOP) CONDITIONS

D. H. Nguyen

ABSTRACT

The failure of carbide fuels in the Fast Test Reactor (FTR) under Transient Overpower (TOP) conditions has been examined. The Beginning-of-Cycle Four (BOC-4) all-oxide base case, at $.50/sec ramp rate was selected as the reference case.

A coupling between the advanced fuel performance code UNCLE-T and HCDA Code MELT-IIIA was necessary for the analysis. UNCLE-T was used to determine cladding failure and fuel preconditioning which served as initial conditions for MELT-III calculations. MELT-IIIA determined the time of molten fuel ejection from fuel pin. In the transient analysis, the UNCLE-T gap conductance modeling was modified to account for bond boiling in Na-bonded fuel elements. A new subroutine was added to MELT to calculate carbide fuel gap conductance. Excellent agreement was obtained between UNCLE-T and MELT-IIIA thermal transient calculations up to fuel melting (UNCLE-T did not handle fuel melting).

The He-bonded carbide fuel led the accident followed by the Na-bonded carbide fuel. The oxide fuel at the highest power level failed next. The He-bonded carbide fuel failed closer to the core midplane (∿10 cm above), the oxide fuel near the top, with the Na-bonded carbide fuel at a location in-between.

In Na-bonded elements, the loss-of-bonding by boiling would cause surface fuel to melt, but molten fuel slumping on cladding would not cause cladding meltthrough, so long as sodium coolant temperature remains below boiling.

THIS PAGE

WAS INTENTIONALLY

LEFT BLANK

FIGURES

Figure		Page
1	Fuel Surface Axial Temperature	3
2	Fuel Cladding Gap and Conductance	5
3	Comparison of Radial Temperatures at Core Node 11 (18 Equal Core Nodes)	6
4	Cladding Inner Surface and Coolant Axial Temperatures	7
5	Axial Fission Gas Retention in Carbide Fuel	8
6	Radial Fission Gas Retention in Carbide Fuel	10
7	Axial Cladding Swelling	11
8	Circumferential Stress in Cladding Outer Ring	12
9	Circumferential Strain in Cladding	13
10	Section-Wise Maximum Cladding Damage Parameters at Failure Time for the He-bonded Pin	17
11	Cladding Maximum Damage Parameter History	18
12	Illustration of the Differential Volume Condition for Fuel Breakup	21
13	Gap Conductance in Carbide Fuel Inner Cladding and Coolant	23
14	Inner Cladding and Coolant Temperature Histories (He-bonded Pin)	24
15	Fuel Surface Temperature History (Na-bonded Pin)	25
16	Radial Temperatures in Na-bonded Pin at Two Different Times Following Bond Boiling	26
17	Illustration of Molten Fuel Cladding Contact	30
18	Variation of Cladding Outer Surface Temperature with Sodium Temperature (T_I = 1941°K)	32
19	Radial Cladding Temperature on Contact with Molten Fuel	33

THIS PAGE

WAS INTENTIONALLY

LEFT BLANK

TABLES

Table		Page
1	Comparison Between Some TREAT Tests and Carbide Fuel in this Study	37
2	Summary of TREAT Tests on Carbide Fuel Elements	38

I. INTRODUCTION

The FFTF irradiation program includes early carbide fuel tests of less than subassembly size. Before carbide fuels can be loaded, their response to transient conditions of the FTR must be examined. This work attempts to determine the key failure parameters (time and location) of carbide fuels under the $.50/sec TOP conditions in the FTR.

We consider a test assembly replacing an oxide fuel subassembly at a location in the FTR row 3. It is a multi-duct grid-spaced assembly, composed of 19 He-bonded pins and 18 Na-bonded pins, and surrounded by 90 oxide pins. The He-bonded pins have a fuel density of 81% TD and a diametrical gap of 0.015 cm, while the Na-bonded pins' density and gap are 98% TD and 0.091 cm, respectively. Both types of pins have an OD of 0.94 cm. Cladding material is 316SS, 20%CW.

The case considered was a $.50/sec TOP accident in the FTR BOC-4 core [1], in which fuel at the location considered had been irradiated for 165 days under a steady state power of 384 MW. A coupling between the advanced fuel performance code UNCLE-T [2] and the HCDA code MELT-IIIA [3] was necessary for the fuel failure analysis. At the time of this analysis, UNCLE-T is the only calibrated advanced fuels code. But UNCLE-T did not handle fuel melting, and so the pin behavior beyond melting was calculated by MELT-IIIA. The transient power history, an UNCLE-T input, was also computed by MELT-IIIA, taking into account feedbacks from sodium density change, Doppler broadening and fuel motion, if any. UNCLE-T preconditioned the fuel for 165 days, before starting the transient.

II. CARBIDE FUEL PRECONDITIONING CALCULATIONS

Carbide fuel preconditioning was calculated by UNCLE-T and the results coupled to MELT-IIIA as initial conditions of the transient calculations. For the BOC-4 Base Case, fuel at location considered had been irradiated for 165 days. The actual loading schedule of carbide fuel may vary its irradiation time prior to the transient, but this assumption provided a case study of irradiated carbide fuels.

Figures 1 through 9 summarize the thermal and mechanical conditions of fuel and cladding after 165 days of irradiation. At this time, the burnup in He-bonded pins ranged from 1.546 a/o in the top axial section to a peak value of 2.896 a/o in Section 4 (corresponding to axial levels 13 and 14 in MELT). In Na-bonded pins, the lowest burnup of 1.448 a/o occurred also at the top section and the peak burnup at Section 4 was 2.712 a/o.

1. Thermal Performance

The results of thermal analysis will be first examined. The temperature fields shown in Figures 1, 3, and 4 have been interpolated to correspond to MELT-IIIA node structure. Whenever possible, the results for oxide fuel from SIEX [4] and STEADY [3] calculations are also included for comparison.

Figure 1 shows the fuel surface axial temperature. The Na-bonded carbide pin operated at several hundred degrees (K) cooler than both the He-bonded carbide pin and the oxide pin. Remarkably, the fuel surface of the He-bonded carbide pin was hotter than that of the oxide pin, which also has a He-bond, although the radius of the latter was much smaller (0.257 cm versus 0.4115 cm cold radii). This is believed to be due mainly to the high thermal conductivity of carbide fuel which enhances the transport of heat to the outer region. The axial variation in the He-bonded carbide pin was quite similar to that of the oxide pin, with a depression in the middle sections due to better gap conductance there. This similarity in fuel

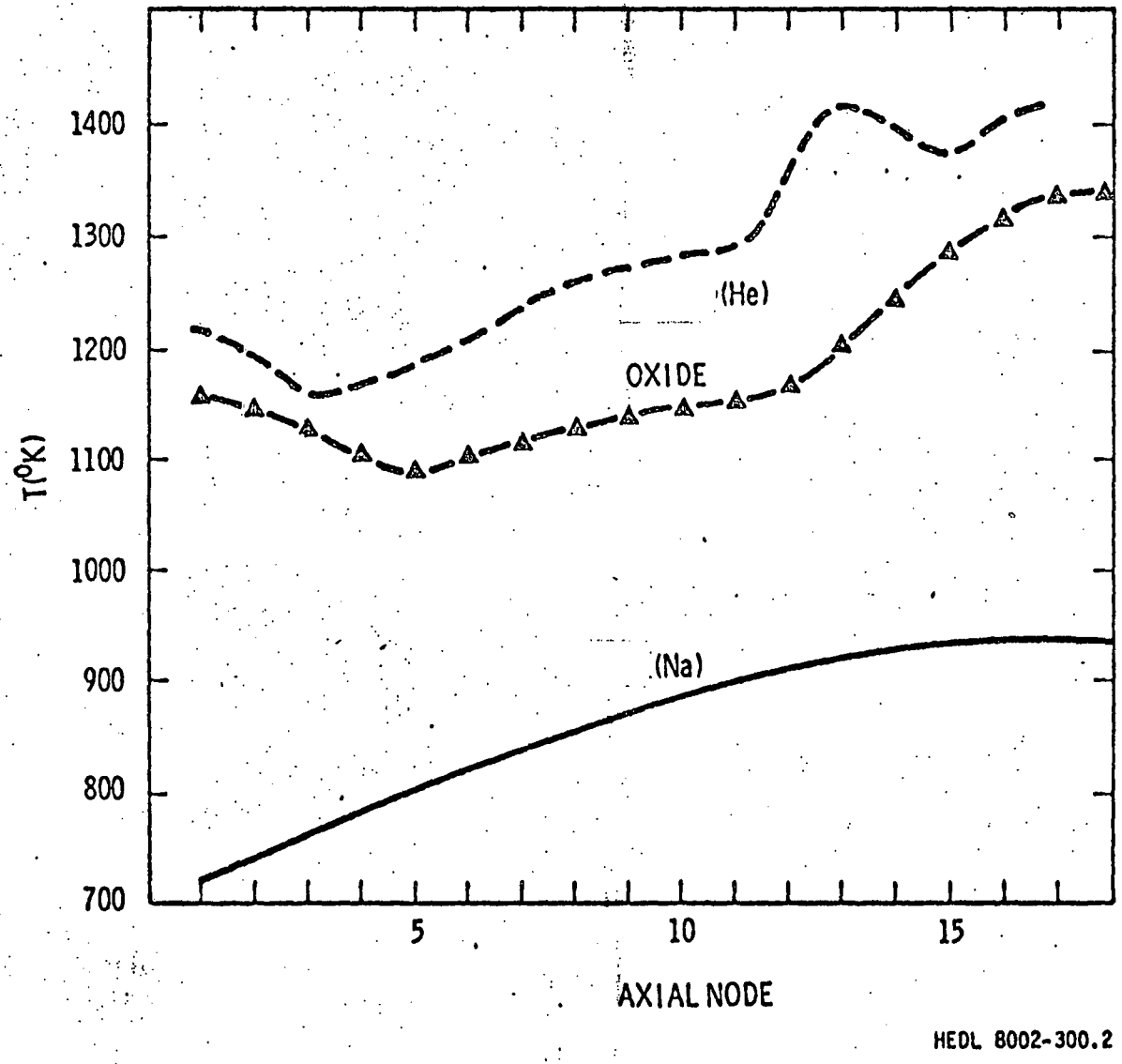

FIGURE 1. Fuel Surface Axial Temperature.

surface temperatures resulted from a similar behavior of the fuel-cladding gap and gap conductance, shown in Figure 2. The gap was closed at the middle sections of the oxide and He-bonded carbide pins. By contrast, the gap remained open at all sections of the Na-bonded carbide pin; its small axial variation in gap conductance resulted in a monotonically increasing fuel surface temperature shown in Figure 1.

Figure 3 compares the radial temperatures at node 17 (near core midplane) for the three fuel pins, showing the larger gradient for oxide fuel, due to its small thermal conductivity. The high Na-bond conductance resulted in a small temperature difference across the gap in the carbide pin.

In Figure 4, it is seen that the cladding inner temperatures are comparable for both carbide pins, but this temperature is lower for the oxide pin. This was caused partly by the high fuel surface temperature in the He-bonded carbide pin and by the large gap conductance in the Na-bonded pin, and partly by the somewhat higher exit coolant temperature than in the oxide channel. This higher exit coolant temperature was calculated by W-ARD[5] and used as a boundary condition in the current UNCLE-T calculations.

2. Restructuring and Fission Gas Information

The fact that no fuel restructuring was calculated is consistent with current irradiation experience, which indicates that carbide fuel restructuring is significant only at a linear rating of 61 kW/ft or higher.[6]

For mechanical analysis, fuel was divided into 5 structural rings, and cladding into 2. Figure 5 shows the axial distribution of total fission gas retained (moles) in several rings. There was a large amount of fission gas retained along the mid-core sections, because of higher fission gas generation there, but still low release at the operating fuel temperatures.

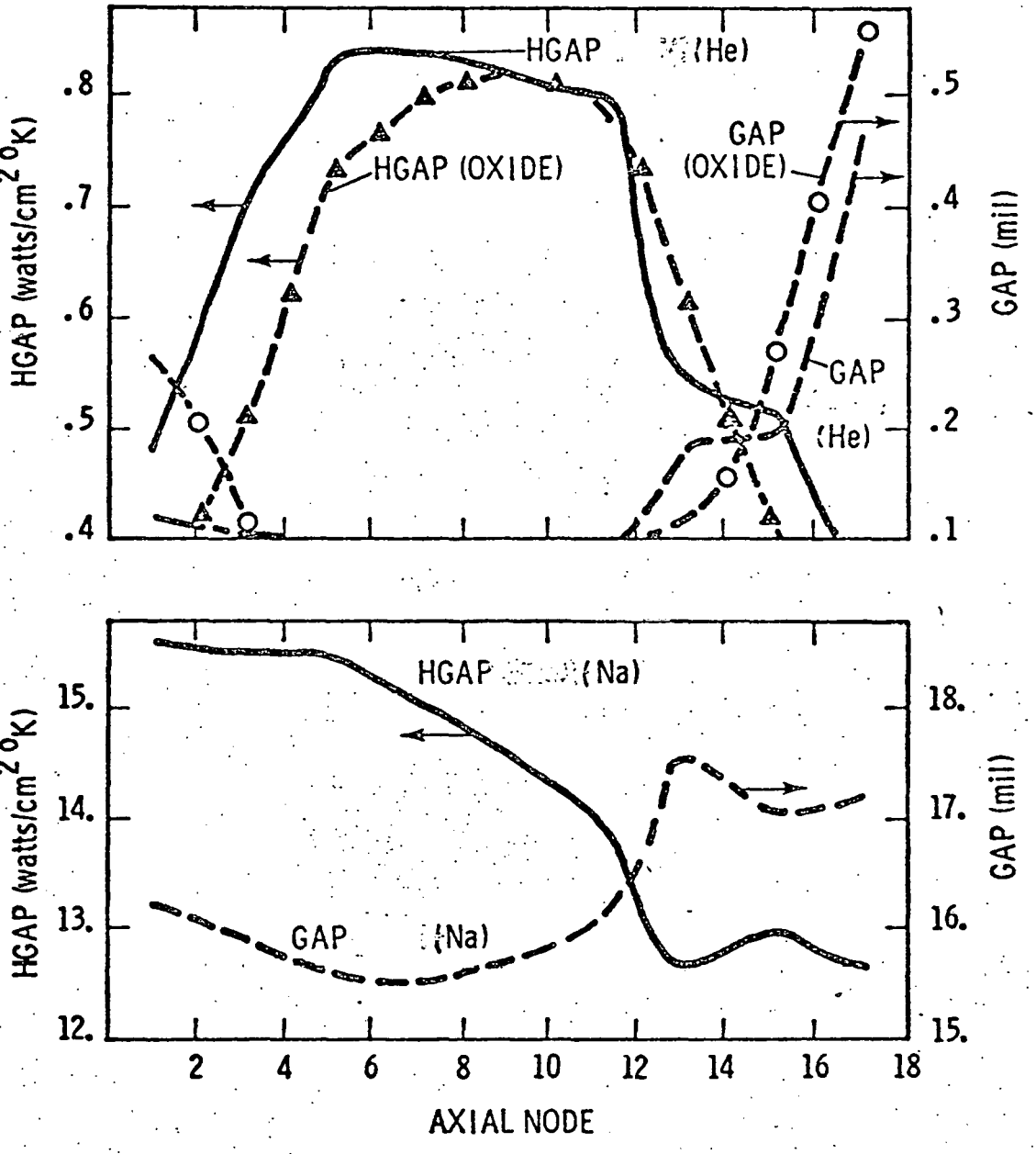

HEDL 8002-0 300.3

FIGURE 2. Fuel Cladding Gap and Conductance.

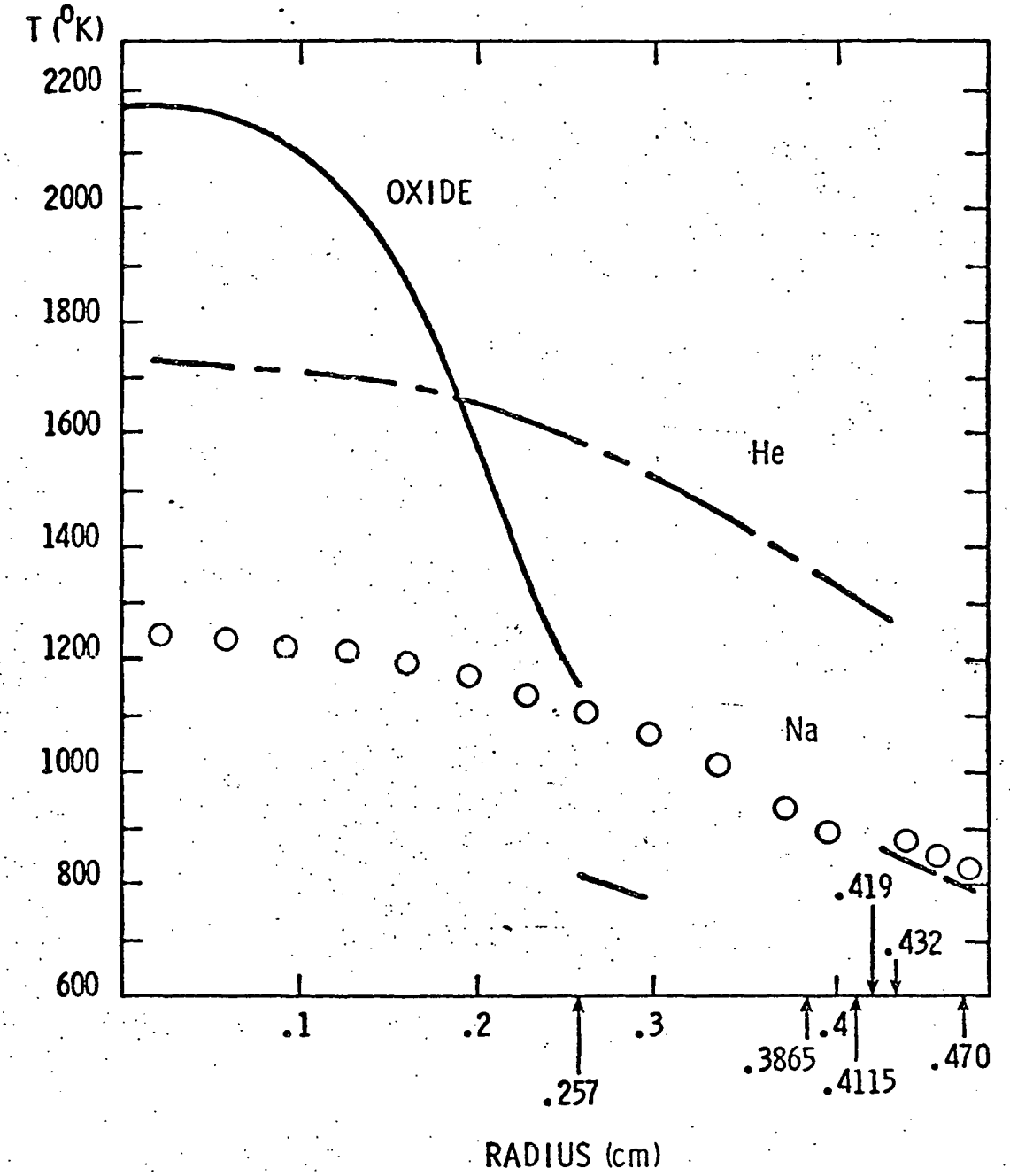

FIGURE 3. Comparison of Radial Temperatures at Core Node 11 (18 Equal Core Nodes).

HEDL 8002-300.5

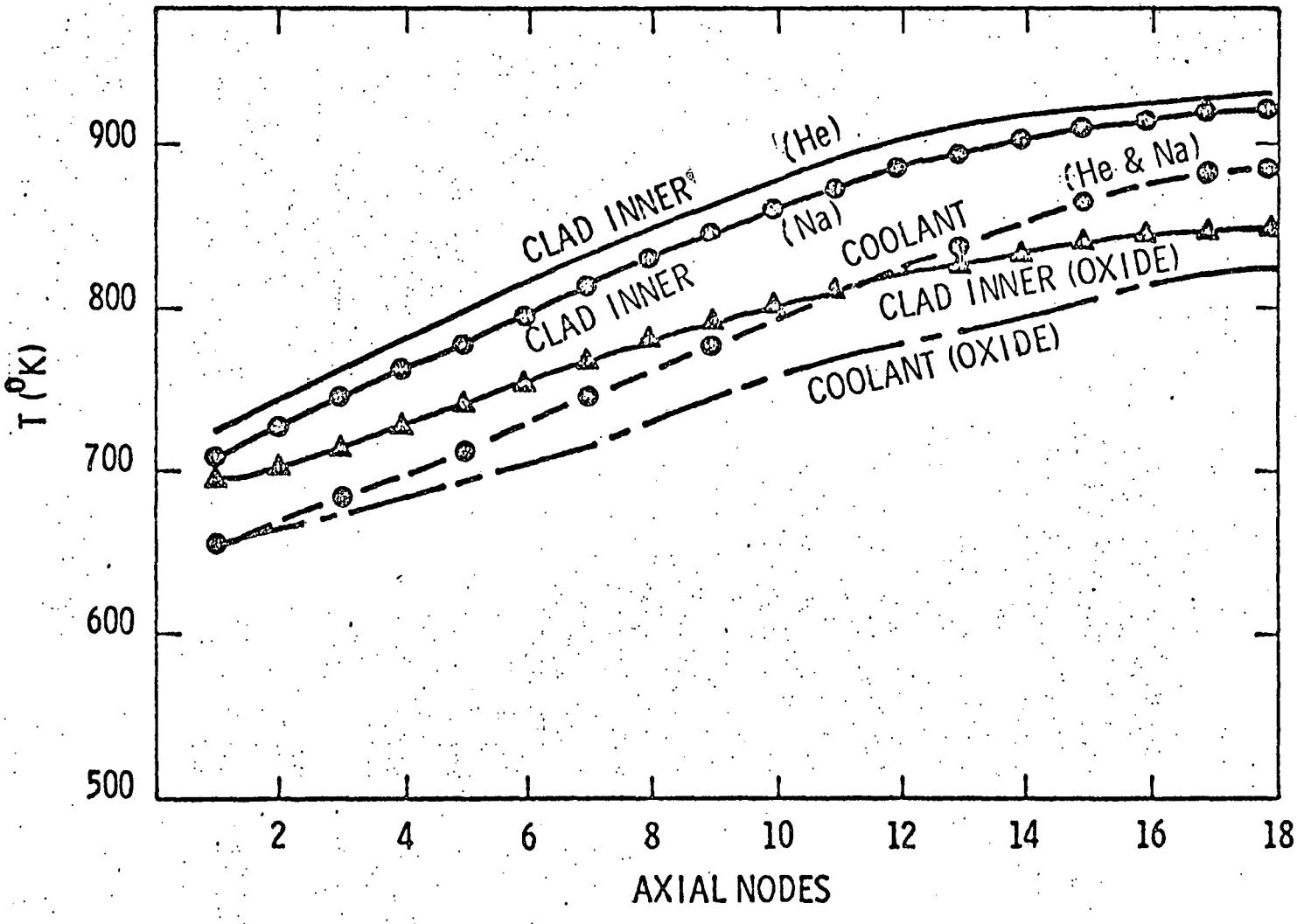

FIGURE 4. Cladding Inner Surface and Coolant Axial Temperatures.

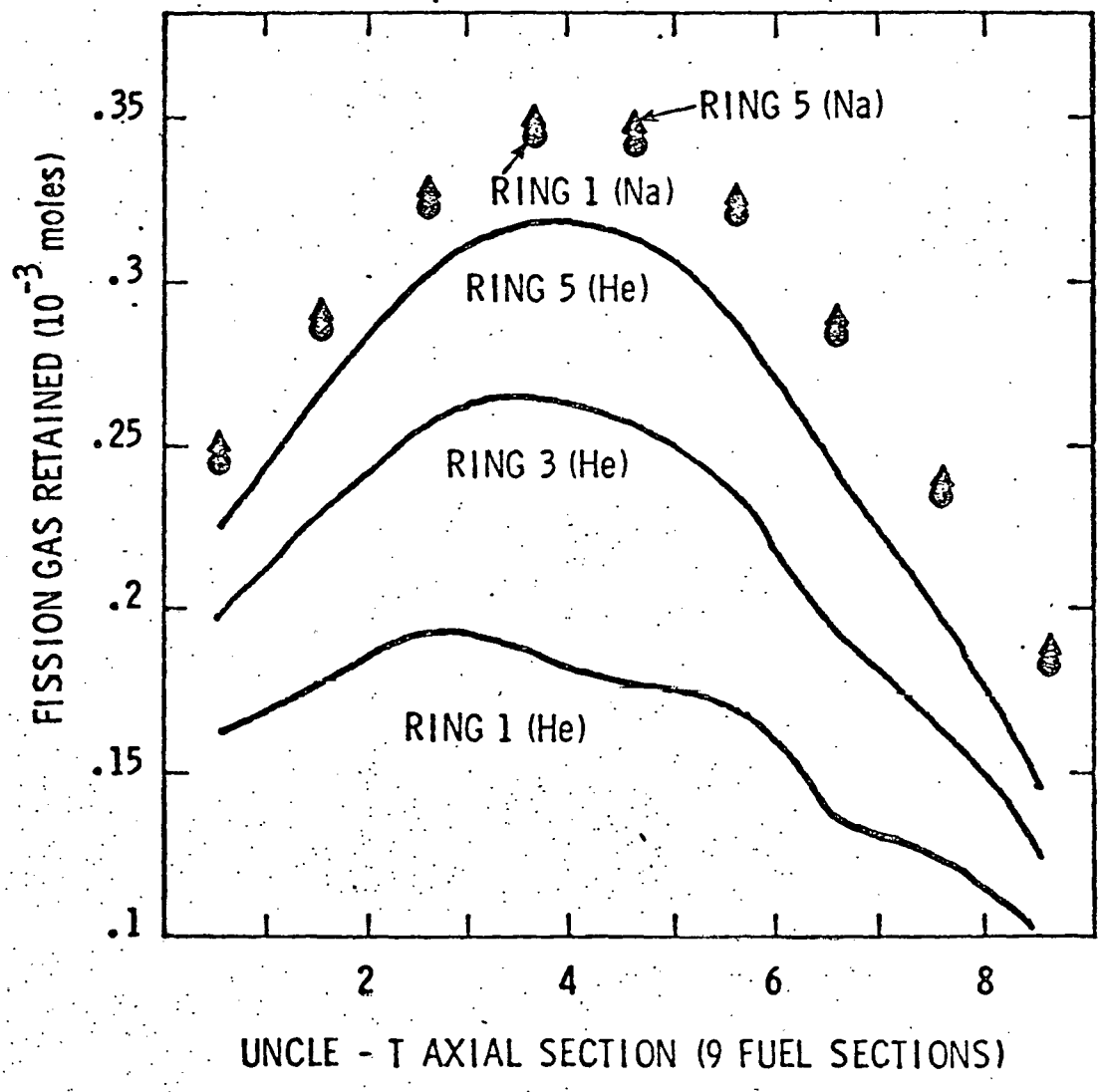

FIGURE 5. Axial Fission Gas Retention in Carbide Fuel.

Figure 6 does show less fission gas retained in hot fuel at the central region. Since Na-bonded fuel operated at much lower temperatures, its fission gas retained was essentially the same throughout the fuel cross section. At the end of the preconditioning period (165 days), 26.6% of total fission gas generated were released in He-bonded pins, while only 0.3% were released in Na-bonded pins. By contrast, 57.28% of fission gas were released in the oxide pin, as calculated by SIEX.

Some remarks should be made concerning the flat radial fission gas retention in the Na-bonded pin shown in Figure 6. A strong radial gradient of fission products concentration was observed in post-irradiation examination of the TREAT test SC3 of a Na-bonded element.[17] This radial dependence of fission products concentration in SC3 was believed to be a characteristic of a severe steady-state irradiation conditions causing the fission products to migrate outward. The Na-bonded pins considered in this study did not undergo a severe preconditioning period and so the fission products gradient was expected to be small, as calculated by UNCLE-T.

3. Mechanical Performance

For both Na-bonded and He-bonded carbide pins, cladding swelling (Figure 7) reached a peak at Section 7 (corresponding to axial levels 19 and 20 in MELT). This peak occurred at a cladding temperature of about 880 K and a fluence of 6×10^{22} (neutrons/cm^2), and was a normal behavior of 316 SS, 20% CW. Remarkably, the oxide pin did not suffer a peak cladding swelling because its cladding had nowhere reached this critical temperature. A close look at the swelling of each cladding ring revealed that in Section 7, the outer ring sustained more swelling than the inner ring, resulting in a compressive hoop stress in the outer ring, shown in Figure 8.

The He-bonded pin generally sustained more strain than the Na-bonded pin (Figure 9). At the sections where strain was high, the gap had closed, leading to the conjecture that the higher strain in the He-bonded pin was probably the result of a fuel-cladding mechanical interaction (FCMI). In

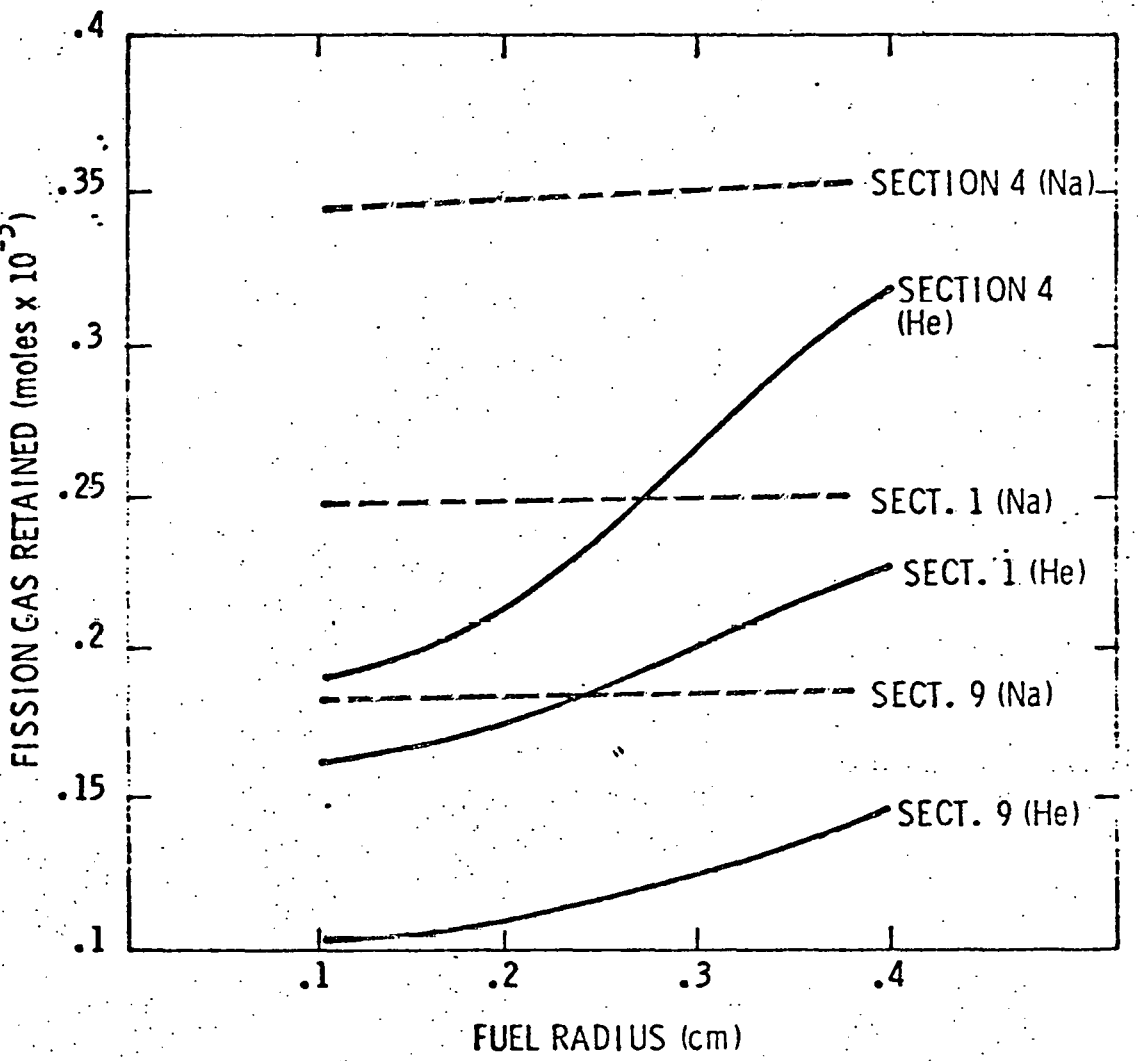

FIGURE 6. Radial Fission Gas Rentention in Carbide Fuel.

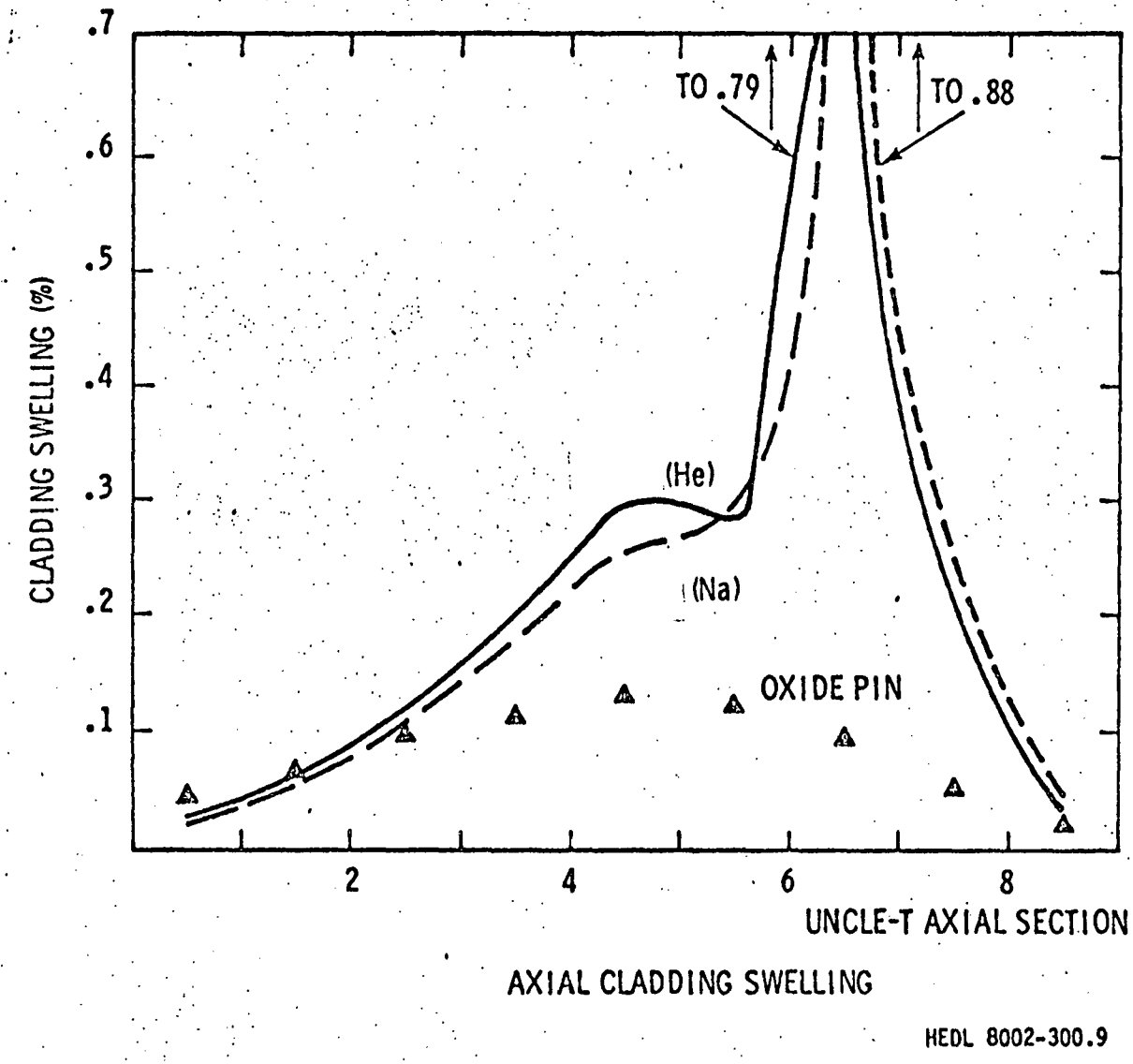

FIGURE 7. Axial Cladding Swelling

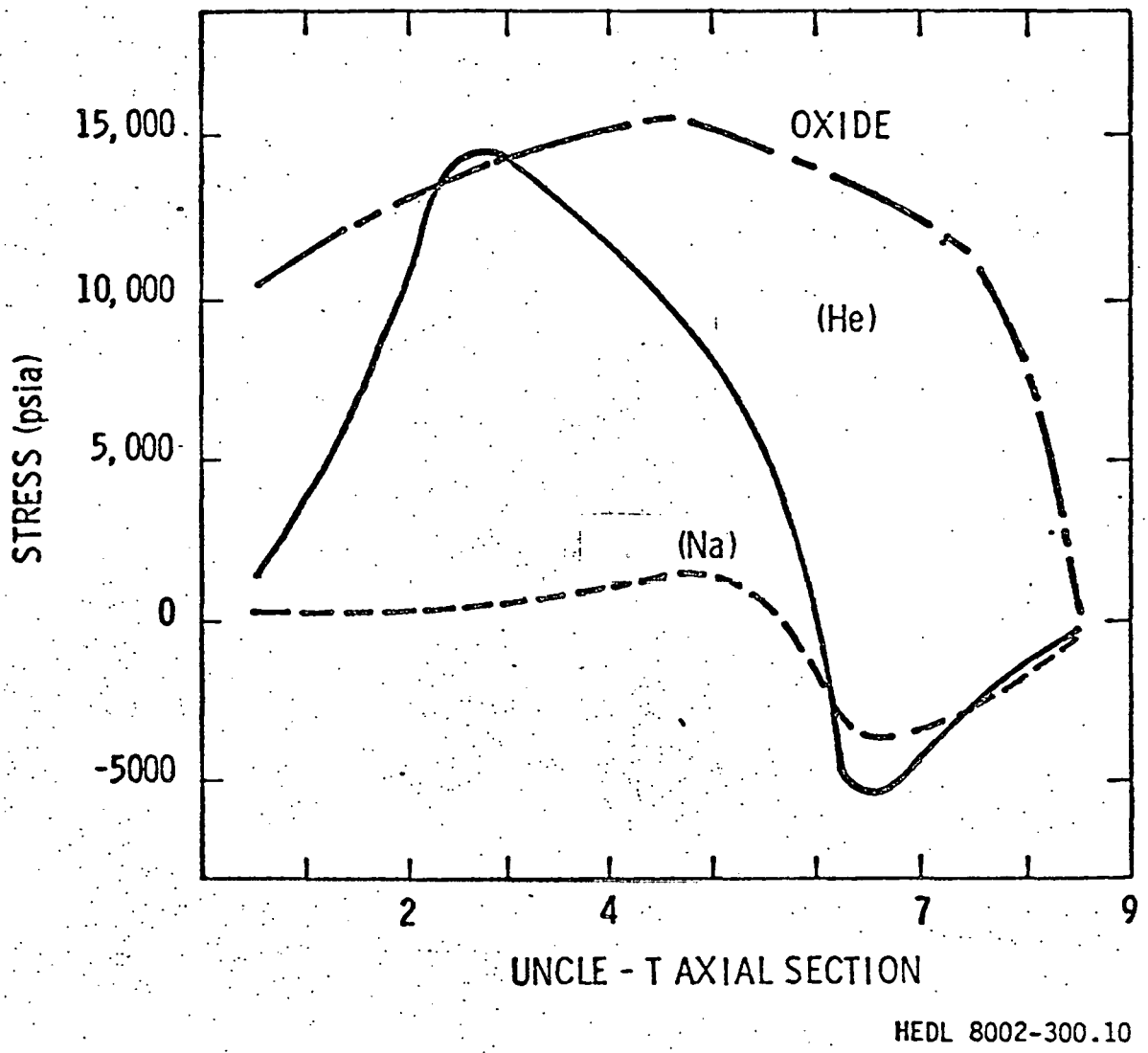

FIGURE 8. Circumferential Stress in Cladding Outer Ring.

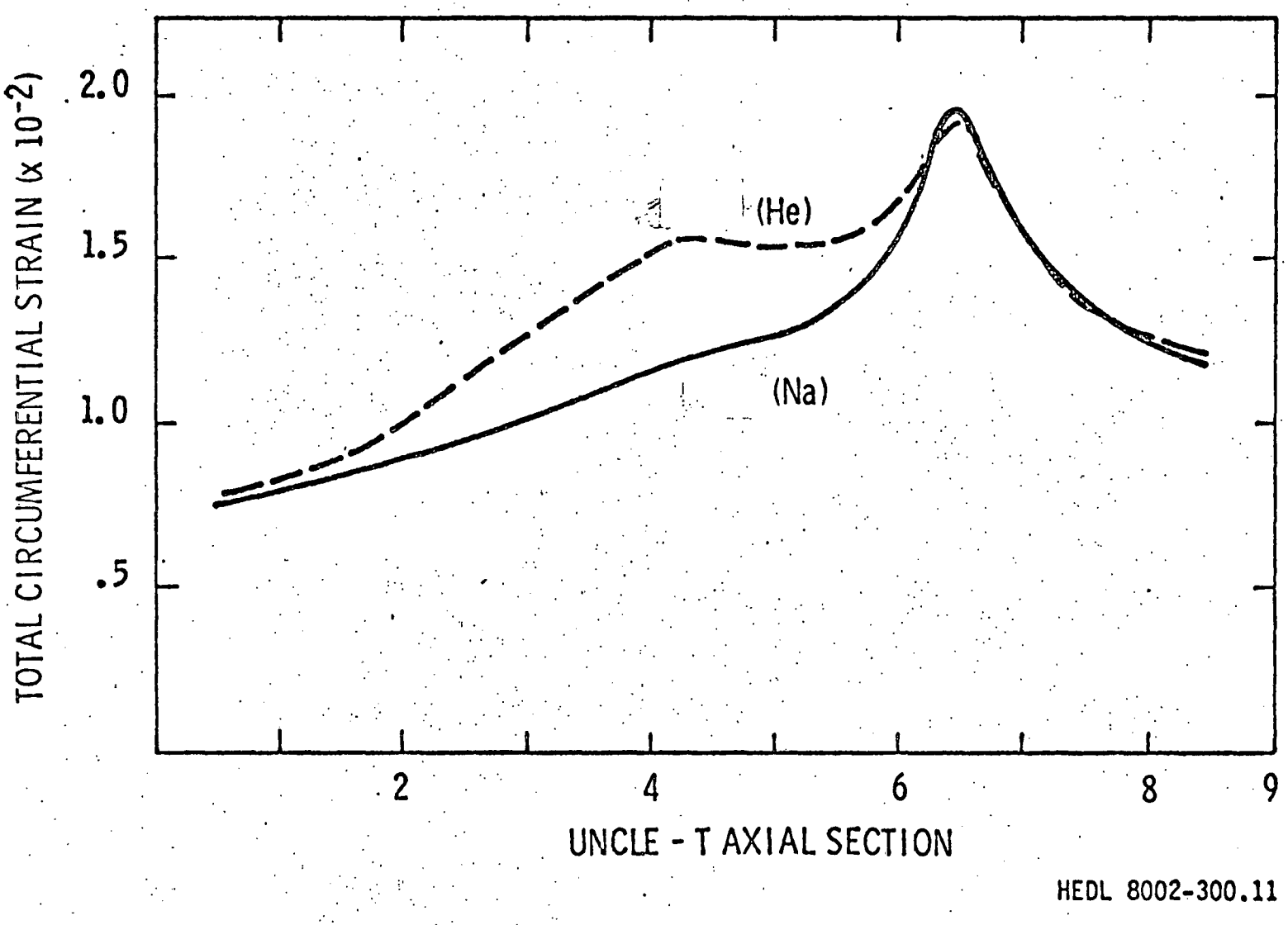

FIGURE 9. Circumferential Strain in Cladding.

Figure 9, the circumferential strain also exhibits a peaking in Section 7 of both Na-bonded and He-bonded pins. This peaking cannot be explained by local FCMI, because the gap was still open for the Na-bonded pin. It was likely caused by the temperature-induced swelling noted earlier.

The results discussed above indicated that UNCLE-T appears to yield reasonable predictions on thermal and mechanical steady-state performance for carbide fuel, inasmuch as these predictions, in general, compare favorably with experience obtained from EBR-II and foreign carbide fuel irradiation programs, as reported in the Tucson and Monterey International meetings on Advanced Fuels.[8,9]

III. DETERMINATION OF FUEL FAILURE

In TOP-HCDA analysis, molten fuel injection into coolant channel is the important event of fuel failures. Depending on the accident conditions, cladding breaching could take place prior to or simultaneously with molten fuel ejection. In the former situation, the internal pin pressure required to break-up the solid fuel annulus surrounding the central molten region would be smaller than if cladding integrity is still maintained. Since the large carbide fuel thermal expansion enhances the probability of a cladding failure prior to fuel melting, UNCLE-T was first used to examine cladding performance. UNCLE-T had the necessary carbide fuel modeling and used the life-fraction rule to determine cladding damage. Cladding was divided into concentric rings and the cumulative damage fraction DMG was determined by the equation:

$$DMG = \sum_{j=i}^{J} \left[\Delta t / tr \left(\bar{\sigma}_\theta , T \right) \right]_j \qquad (1)$$

where Δt is the time increment and tr is the time to rupture evaluated at average hoop stress $\bar{\sigma}_\theta$ and average temperature T of the cladding rings. Failure was assumed when $DMG \geq 1$. The reactor power history, an UNCLE-T input, was computed by MELT-IIIA.

UNCLE-T determined whether cladding would fail. But cladding might fail prior to fuel melting, which UNCLE-T did not handle. So, prediction of pin behavior following fuel melting was based on MELT-IIIA calculations, as was the determination of the time and location of molten fuel ejection. UNCLE-T calculations of fuel preconditioning served as initial conditions to MELT calculations.

1. Failure of He-Bonded Carbide Fuel

Figure 10 shows the section-wise maximum cumulative damage fraction in the He-bonded element (channel #8) at 1.91 sec into the transient. Clearly Section 6 (corresponding to MELT core nodes 11 and 12) had reached the condition for cladding breaching at this time. Figure 11 shows that once the cladding damage began to accumuate in the He-bonded pin, it reached the breaching threshold in a very short time. For subsequent HCDA analysis, the location of failure was conservatively assumed to be at the MELT core node 11 (~10 cm above core midplane). Because the fuel-cladding gap was closed at the onset of the transient, it was assumed that cladding failure was stress-induced and caused mainly by differential thermal expansion and fuel swelling by fission products. Since UNCLE-T had correctly predicted cladding breaching for the TREAT test HC3,[10] there was some guarded confidence in the time of failure as determined. Post-test examination of the HC3 element confirmed that cladding breaching was in the form of longitudinal cracks. Information on the time and location of initial cladding breaching was not available. It was originally thought that fuel melting did not occur in HC3 test, but more recent PIE indicated evidence of fuel melting,[11] although it was not known whether this happened after or prior to cladding failure.

At the time of cladding failure in the He-bonded element, the maximum fuel temperature (at axial Section 5, centerline) calculated by UNCLE-T was below melting at 2543°K, although cladding temperature at the failed section was high, at 1188°K. The fuel hot spot did not reach solidus temperature until about 190 msec later, at 2.10 sec into the transient. Upon cladding breaching, hot but solid fuel was exposed to sodium coolant. Based on limited data from the U.S. Run-Beyond-Cladding-Breach (RBCB) program and similar foreign programs,[7] chemical reaction between carbide solid fuel and sodium appeared to be more benign than oxide fuel. It was therefore assumed that no real effect on the HCDA existed until molten fuel motion began. But because of the absence of the central void, no molten fuel motion took place until the solid fuel annulus broke up thereby allowing molten fuel injection into coolant channel.

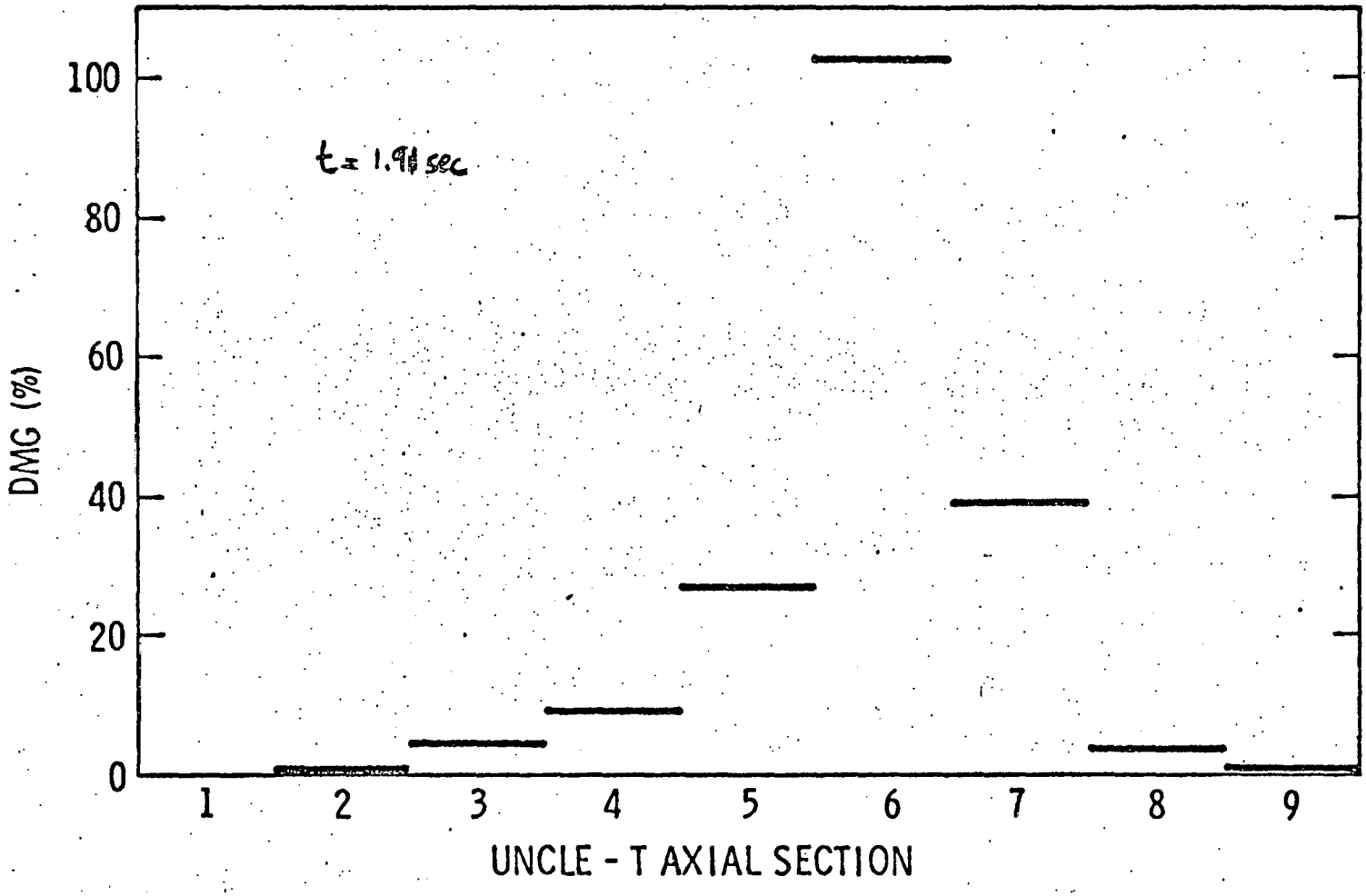

FIGURE 10. Section-Wise Maximum Cladding Damage Parameters at Failure Time for the He-bonded Pin.

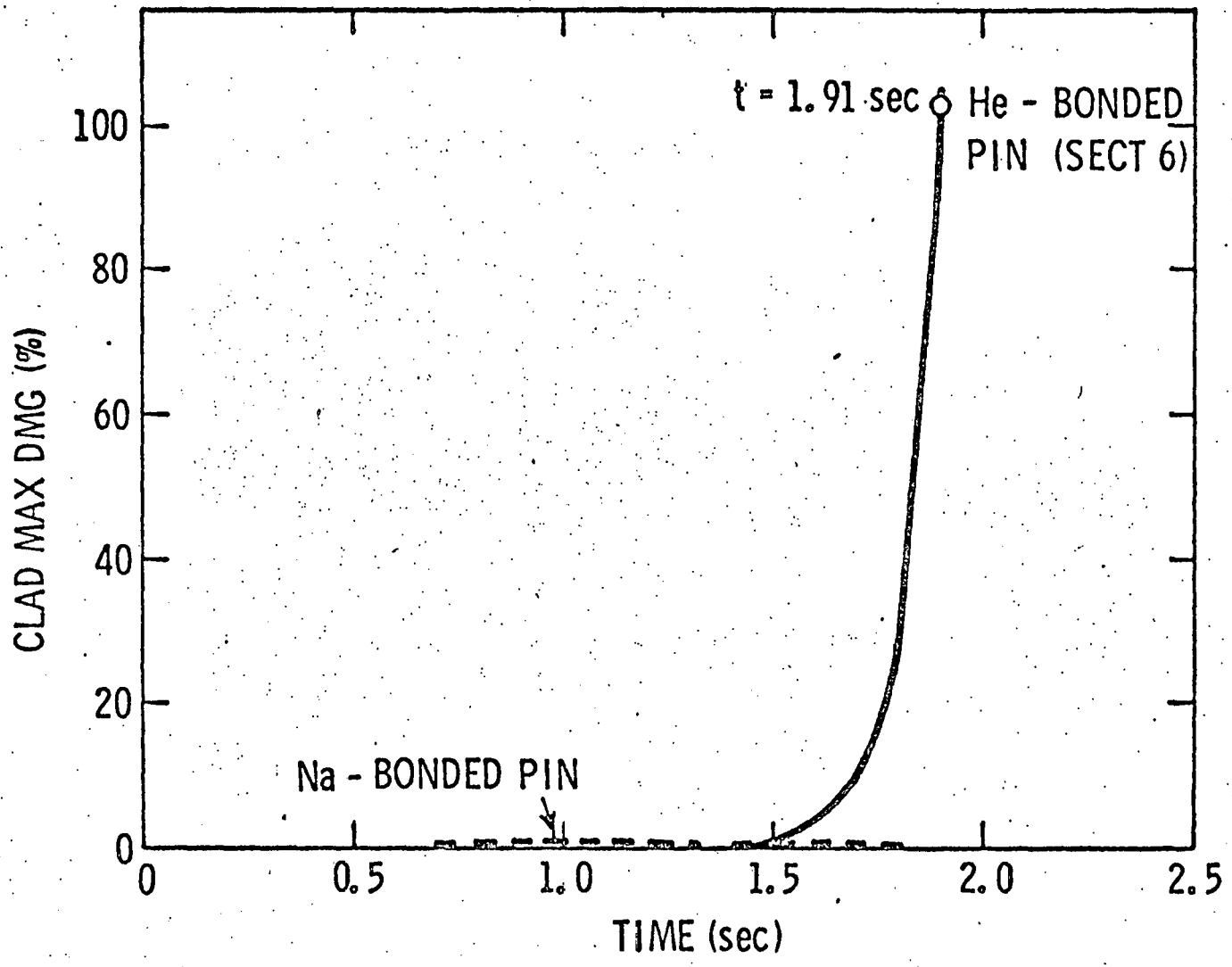

HEDL 8002-300.41

FIGURE 11. Cladding Maximum Damage Parameter History.

In the MELT-IIIA calculations, molten fuel ejection was assumed when the internal pin pressure caused by fission gas release reached a critical value. For FTR oxide fuel, this critical pressure might be taken as that pressure which caused cladding rupture, and determined from a series of cladding transient burst tests[12] to be 7×10^8 dynes/cm^2. Since for the BOC-4 case considered, the fuel-cladding gap was closed at the onset of the transient, it was implied that the internal pin pressure was fully transmitted to cladding. It was also implied that a pressure sufficient to rupture cladding would also break up the remaining solid fuel wall.

There were both similarities and differences between the oxide fuel element and the He-bonded carbide element. The gap was initially closed for both, and the cladding in the carbide element was also 316 SS, 20% cw. However, the carbide element cladding was already breached when fuel melting began, implying that an initial pin pressure sufficient to break up the solid fuel annulus would cause molten fuel ejection. The radius of He-bonded carbide fuel is larger than that of oxide fuel (0.4115 cm versus 0.24765 cm) and so, a conservatively larger break-up internal pressure of 7.7×10^8 dynes/cm^2 was assumed for the carbide element. The effect of a larger pressure is to delay fuel rupture time, allowing thereby a larger amount of molten fuel to be ejected. MELT predicted that this pressure was attained at 2.40 sec into the transient, or about 300 msec following fuel melting. At this time, only about 4% of fuel in the pin was molten. For comparison, under similar transient conditions, it took the oxide pin about 1 sec following melting to reach its break-up pressure, with over 50% molten fuel in the pin. The faster rise in central pin pressure of the carbide fuel element was thought to be caused by a larger fission gas release on fuel melting, and by the absence of the central void.

To insure that fuel break-up took place, a second condition was introduced based on thermal expansion. The condition for such break-up could be stated in terms of the ability of the fuel to accommodate the differential volume thermal expansion on melting. Since there was no central void, the volume

available to absorb thermal expansion came from fuel porosity, crack and fuel-cladding gap, if any. The condition became:

$$\Delta V_{melting} - (V_p + V_c + V_G) > 0 \qquad (2)$$

where $\Delta V_{melting}$ was the increase in fuel volume on melting, and where V_p, V_c, V_G were the volume available from fuel porosity, cracks and fuel-cladding gap, respectively (Figure 12). Clearly, $V_G = 0$ when the gap closed. The He-bonded carbide fuel had a large porosity, about 19%. For oxide fuel, the porosity was not available for thermal expansion absorption, until fuel became weaker at temperatures about 200°K within melting. This was also assumed for carbide fuel. The crack volume was assumed at 3%. At the melting point, the density of carbide fuel was 12.3 gm/cm^3.[13] The density of liquid fuel was computed by the equation.[14]

$$\rho_{liquid} = \frac{12.39}{1 + 9.84 \times 10^{-5} T}, \qquad (3)$$

yielding $\rho_{liquid} = 9.745$ gm/cm^3 at the liquidus temperature. Thus a temperature increase from solidus to liquidus would result in a volume expansion of ~26.2%. MELT calculations indicated that condition (2) was satisfied even earlier than 2.40 sec into the transient, when the internal pin pressure reached 7.7×10^8 dynes/cm^2.

2. Failure of Na-Bonded Carbide Fuel

The results thus far indicated that molten fuel injection into the coolant channel began in the He-bonded channel (channel #8) at 2.40 sec into the transient. Sodium void and fuel motion reactivity following channel #8 failure should be reflected in the power history used in the Na-bonded pin failure analysis. Failure data for channel #8 were thus input in a 9-channel run of MELT-IIIA to determine a new power history for the UNCLE-T failure analysis of channel #9.

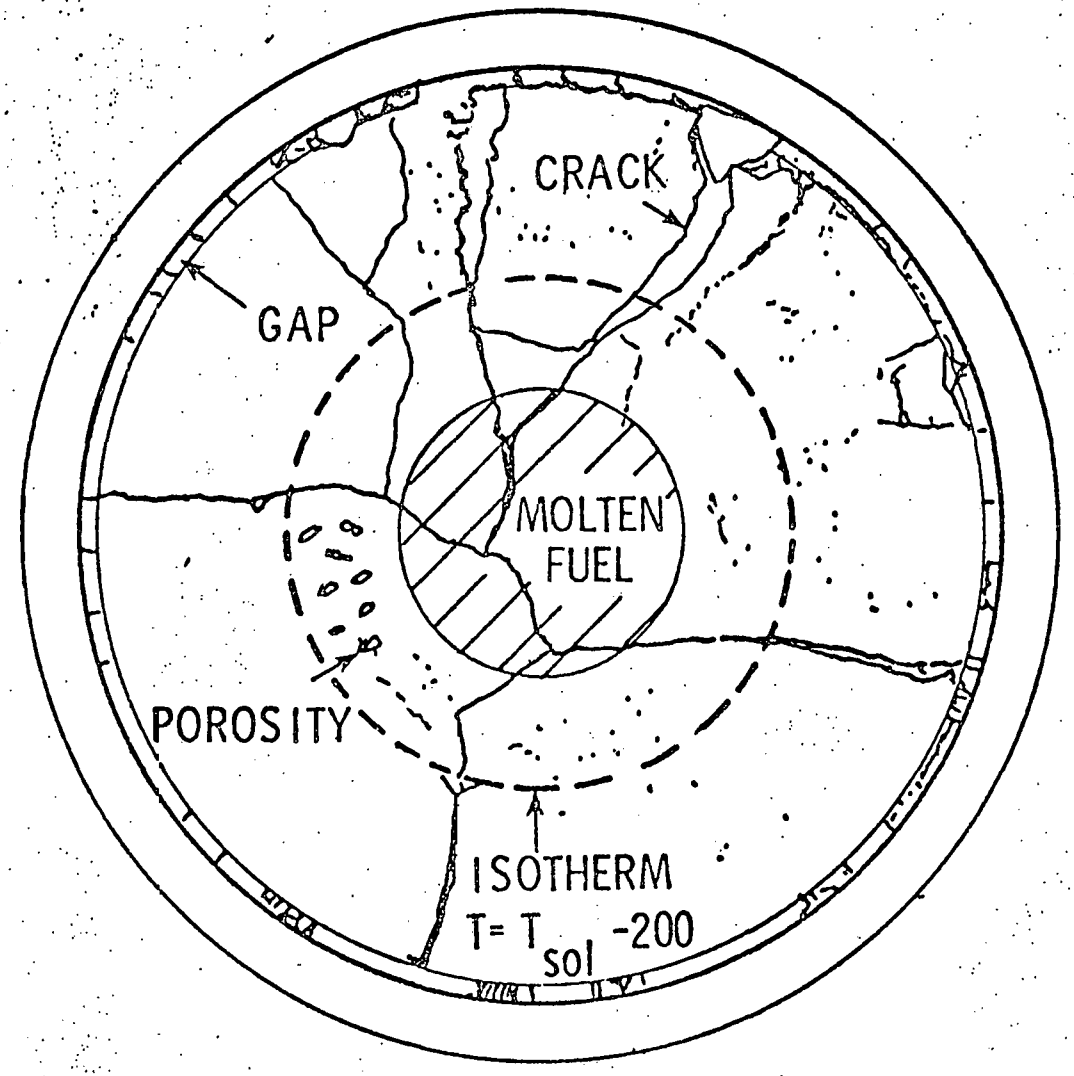

HEDL 8002-300.42

FIGURE 12. Illustration of the Differential Volume Condition for Fuel Breakup.

The subroutine GAPCON of UNCLE-T was modified to include a simplified simulation of loss-of-bonding (LOB) due to bond boiling: the bond was assumed to vaporize upon reaching the saturation temperature at plenum pressure. The sharp discontinuity exhibited in Figure 13 is a consequence of this assumption.

According to UNCLE-T calculations, bond boiling began at Section 8 (MELT core nodes 15 and 16) at 1.900 sec into the transient, and quickly spread along the upper third of the fuel pin. By the time fuel first attained solidus temperature at 2.57 sec, bond boiling had spread along the upper 2/3 of the fuel element. Bond boiling dramatically reduced heat transfer to cladding, such that its temperature dropped while the fuel surface temperature rose quickly (Figures 14 and 15). The fuel-cladding gap, which remained open, kept the hoop stress low, such that cladding never failed according to the life-fraction rule (a maximum DMG of 0.31% was reached in Section 9, at the top of fuel (Figure 11). The fuel temperature along the sections where LOB had occurred continued to rise quickly and due to high thermal conductivity, the radial temperature gradient was dramatically reduced in these sections. Figure 16 depicts this situation at Section 6 (MELT core nodes 11 and 12): the temperature drop across fuel radius decreased from about 800K at the beginning of LOB to about 80K, 0.55 sec later. The fuel surface along this section soon reached solidus temperature at 2.6 sec into the transient. At this time, MELT calculations at core node 12 indicated a centerline temperature of 2600°K and a fuel surface temperature of 2576°K. Since the difference between liquidus temperature (2758°K) and solidus temperature (2575°K) was 183 degrees, a very small fraction (0.73%) of fuel in the Na-bonded pin had melted at this time. The smallest gap size was still at 11 mils, and the stainless steel shroud, at 1783° had melted. The molten shroud might form a low-melting eutectic alloy with surface fuel. The molten eutectic might slump across the gap and contact the cladding, thereby raising the possibility of cladding melt-through.

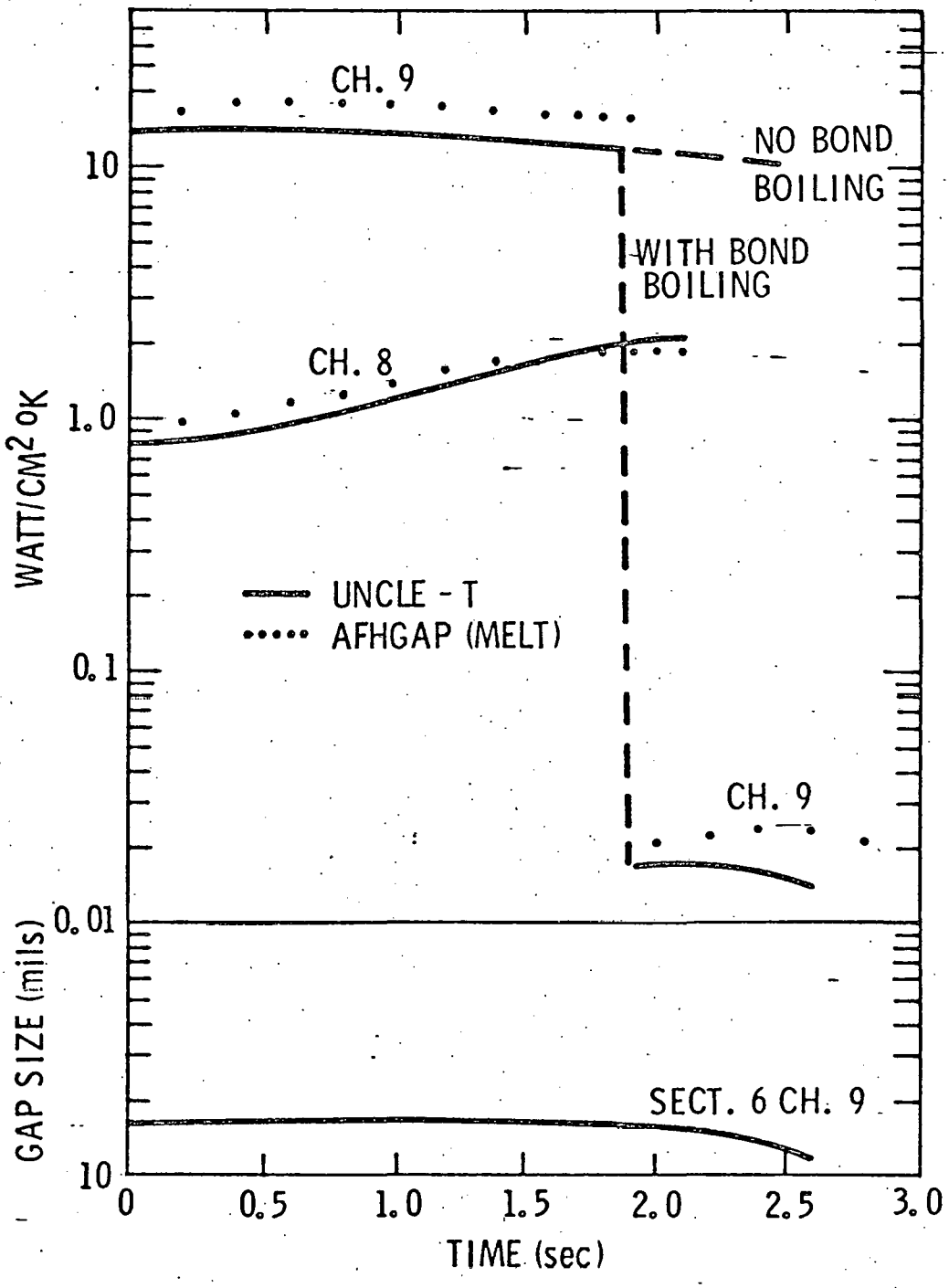

FIGURE 13. Gap Conductance in Carbide Fuel Inner Cladding and Coolant. HEDL 8002-300.29

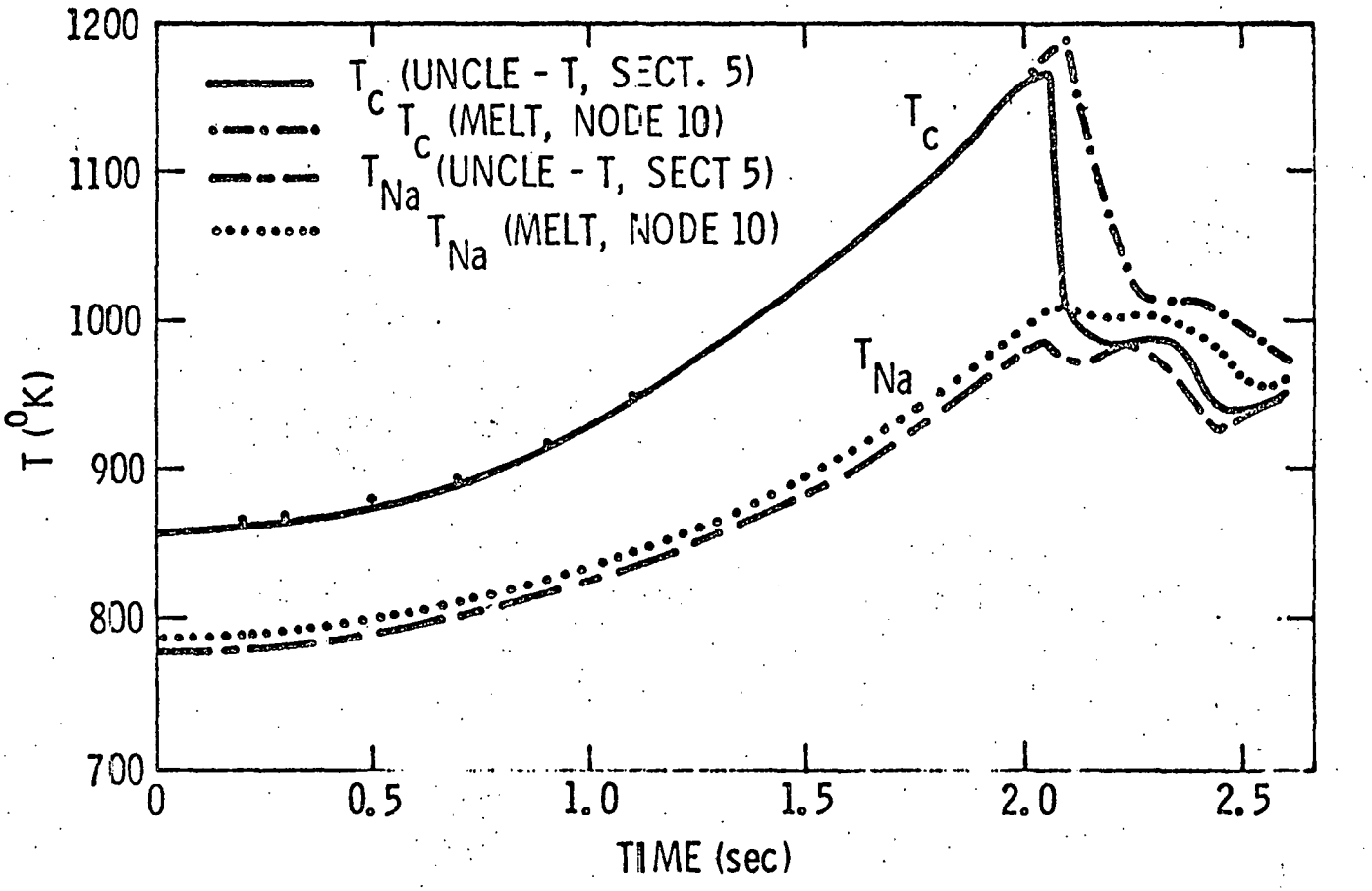

FIGURE 14. Inner Cladding and Coolant Temperature Histories (He-bonded Pin).

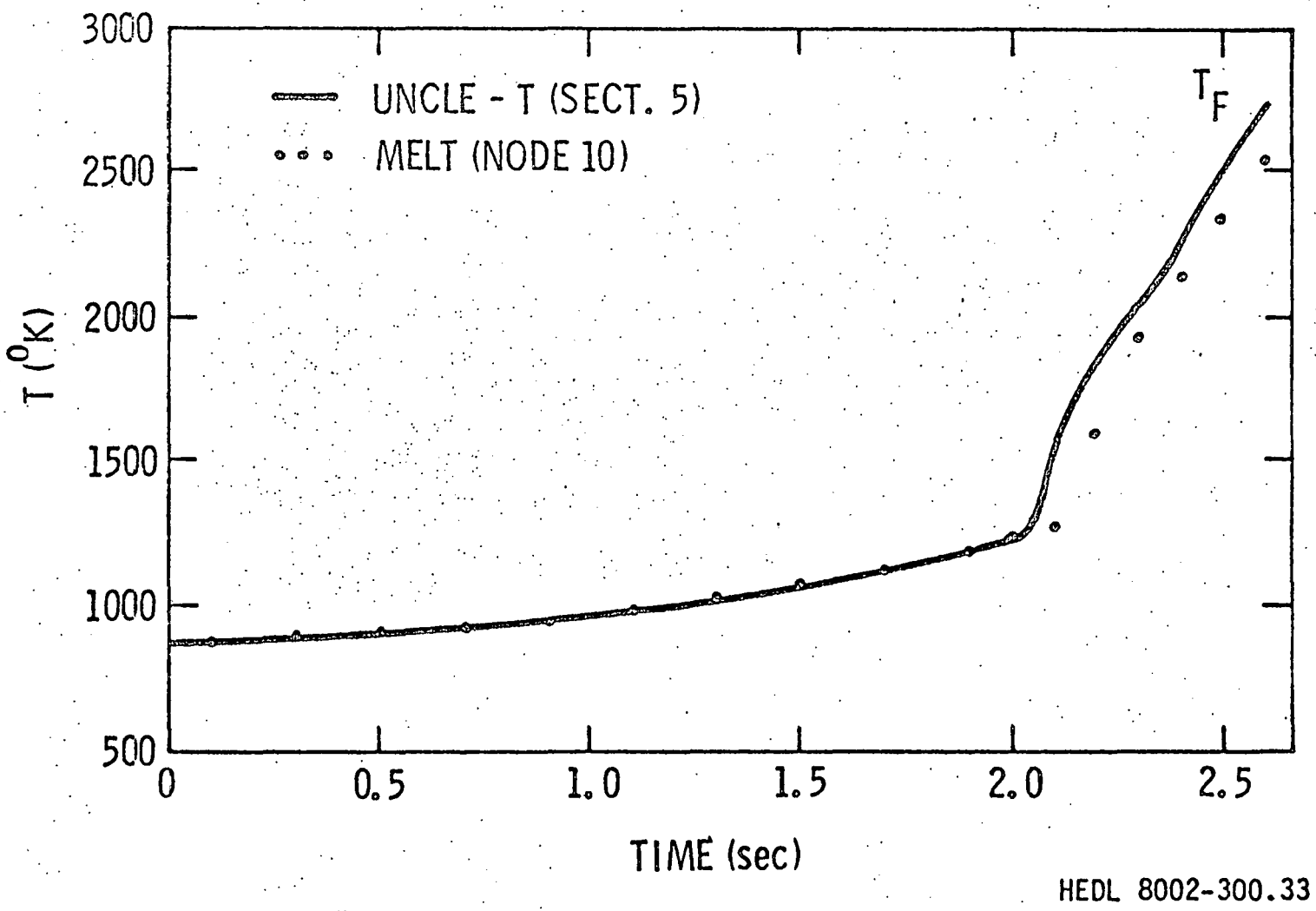

FIGURE 15. Fuel Surface Temperature History (Na-bonded Pin).

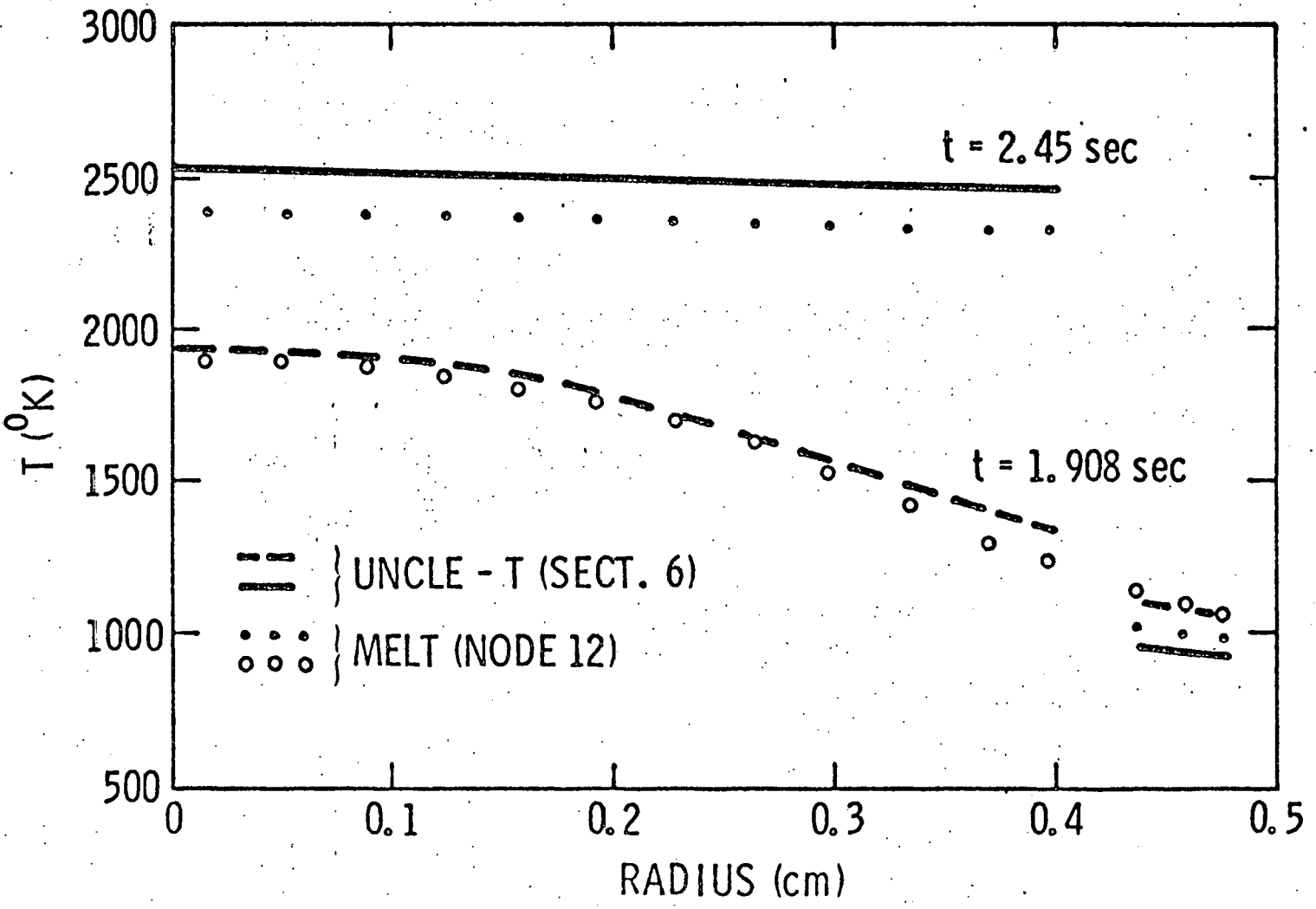

FIGURE 16. Radial Temperatures in Na-bonded Pin at Two Different Times Following Bond Boiling.

Two different approaches were attempted to resolve this question. The first approach used the concept of contact resistance heat transfer between molten fuel and cladding. This method met with only partial success. The second approach used analytic solutions to estimate the cladding temperature distribution under conservative boundary conditions. The results are discussed below.

a. Molten Fuel-Cladding Heat Transfer Through Contact Resistance

Figure 17a depicts the possible configuration of molten fuel-cladding contact. Pockets of gases (Na vapor, fission gas) might be embedded between points of contact. There was no significant contact pressure. The conductance for this case is given by the equation[15]

$$h_c = \frac{1}{L_g}\left[\frac{A_c}{A}\,\frac{2\,k_1k_2}{k_1+k_2} + \frac{A_v}{A}\,k_v\right] \qquad (4)$$

where

L_g = thickness of void space

A_c = contact area

A_v = void area

$A = A_c + A_v$

k_1, k_2, k_v = thermal conducting of molten fuel, cladding and gas in void space, respectively.

Assuming $A_v \ll A_c$ and $k_v \ll k_1$, k_2, the second term in the right-hand-side of Eq. (4) can be neglected. The resulting equation still involves an unknown constant and can only be used parametrically. In MELT-IIIA calculations, the equation was approximated as follows:

$$h_c = \frac{C}{gap} \left(\frac{2 k_1 k_2}{k_1 + k_2} \right) \qquad (5)$$

where C is a constant. For $C > 0.2$, the gap conductance following molten-fuel-cladding contact could become several hundred times larger than that at the previous time step, prior to contact.

This rapid increase in gap conductance caused a convergence problem in MELT temperature calculations. For $C = 0.2$, implying about a hundred-fold increase in conductance, a solution was obtained indicating a rapid increase in cladding temperature which remained nevertheless below melting. This result needed further examination, and a conservative approach was used to estimate the cladding temperature as described in Section (b) below.

A useful result from the method of contact resistance heat transfer was the indication of a decrease in fuel temperature on contact with cladding. Thus, the assumption of a sustained interface temperature T_I (in Section b), is at best conservative. Calculations indicated that along the locations where molten fuel contacted cladding, cyclic variations in fuel and cladding temperatures occurred, with a net upward trend.

b. Analytic Estimate of Cladding Melt-Through

Assuming no contact resistance, the interface temperature T_I between two semi-infinite media suddenly brought into in contact can be calculated by pure conduction solutions[16] as follows:

$$T_I = \frac{T_2 + T_1 \left[(k\rho c)_1 / (k\rho c)_2 \right]^{1/2}}{1 + \left[(k\rho c)_1 / (k\rho c)_2 \right]^{1/2}} \qquad (6)$$

where k, ρ, c are the thermal conductivity, density and specific heat, respectively, and where subscripts 1, 2 refer to molten fuel and cladding, respectively. For a given T_1 and T_2, Eq. (5) yields the maximum interface temperature.

With the further conservative assumption that this interface temperature can be maintained over the cladding thermal response time, the mixed conduction-convection system of Figure 17b can be described by the following simple boundary-value problem. In the cladding, the temperature is determined by the equation:

$$\frac{1}{r}\frac{d}{dr}\left[r\, k_2 \frac{dT_2}{dr}\right] = 0, \tag{6}$$

subjected to the boundary conditions:

$$\begin{aligned} &1.\quad T_2 = T_1 \text{ at } r = r_c \text{ (inner cladding radius)} \\ &2.\quad -k_2 \frac{dT_2}{d_r} = h(T_s - T_{Na}) \text{ at } r = r_s \text{ (outer cladding radius)} \end{aligned} \tag{7}$$

The solution can be obtained as follows:

$$\frac{T_I - T_s}{T_I - T_{Na}} = \frac{hr_s \ln(r_s/r_c)}{k_2\left(1 + \frac{hr_s}{k_2}\ln(r_s/r_c)\right)}, \tag{8}$$

where h is the convective heat transfer coefficient at outer cladding surface.

Equation (8) allows the estimate of cladding surface temperature T_s for given T_I and T_{Na}. At the time of first molten fuel slumping along core node 12,

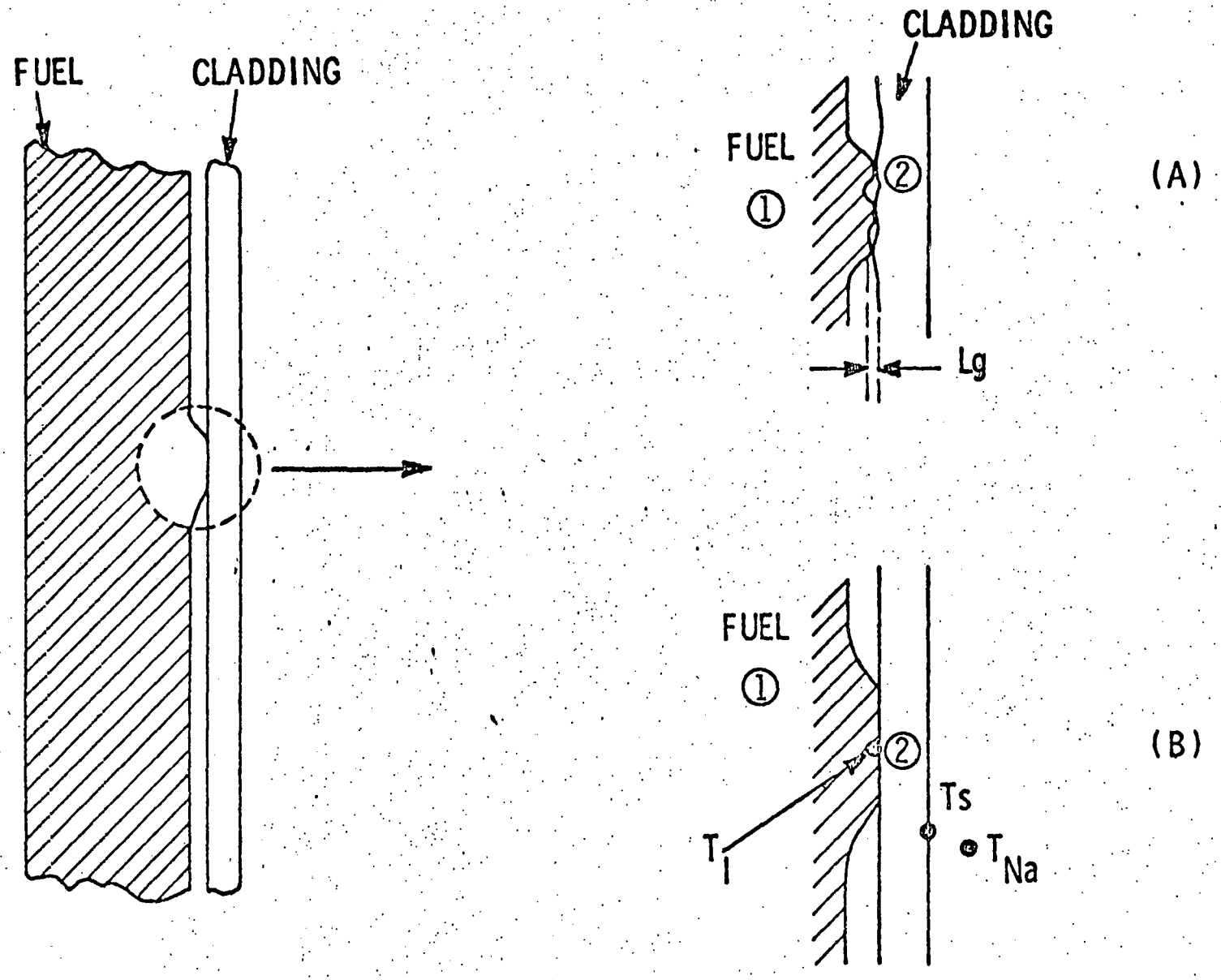

FIGURE 17. Illustration of Molten Fuel Cladding Contact.

MELT calculated a fuel surface and coolant temperatures of 2576°K and 990°K, respectively, yielding T_I = 1941°K (Eq. 5). Figure 18 shows the variation of T_s with coolant temperature, assuming the interface temperature T_I can be maintained over the cladding thermal response time period (~12 msec). For the case considered, cladding outer surface temperature was only 1402°K. Furthermore, cladding melt-through would not occur, so long as sodium coolant temperature remained below boiling (~1312°K at 3.6 atm.) Figure 18 does not apply beyond sodium boiling.

The depth of cladding melting can also be estimated, by obtaining the solution to Eqs. (6) and (7), with the boundry condition (2) replaced by the condition

$$T_2 = T_s \text{ at } r = r_s$$

Thus,

$$T_2(r) = T_I + \frac{(T_s - T_I)}{\ln (r_s/r_c)} \ln (r/r_c) \qquad (9)$$

where T_s is computed from Eq. (8). Figure 19 shows such distribution at MELT node 18 (core node 12) when molten fuel-cladding contact first occurred. The depth of cladding melting was only less than one half of cladding thickness.

c. Pin Failure

At the time fuel surface first reached the solidus temperature (2.61 sec along core node 12), only 0.73% of fuel had melted. The total fuel volume increase on melting was small, a large gap remained (~11 mils), and the condition of Eq. (2) was not satisfied at this time. At the next time step (2.62 sec), molten fuel contact could heat the inner cladding node to melting point, and cladding strength would have been reduced. The internal pin pressure had reached the breakup point (7.7×10^8 dynes/cm^2). Cladding

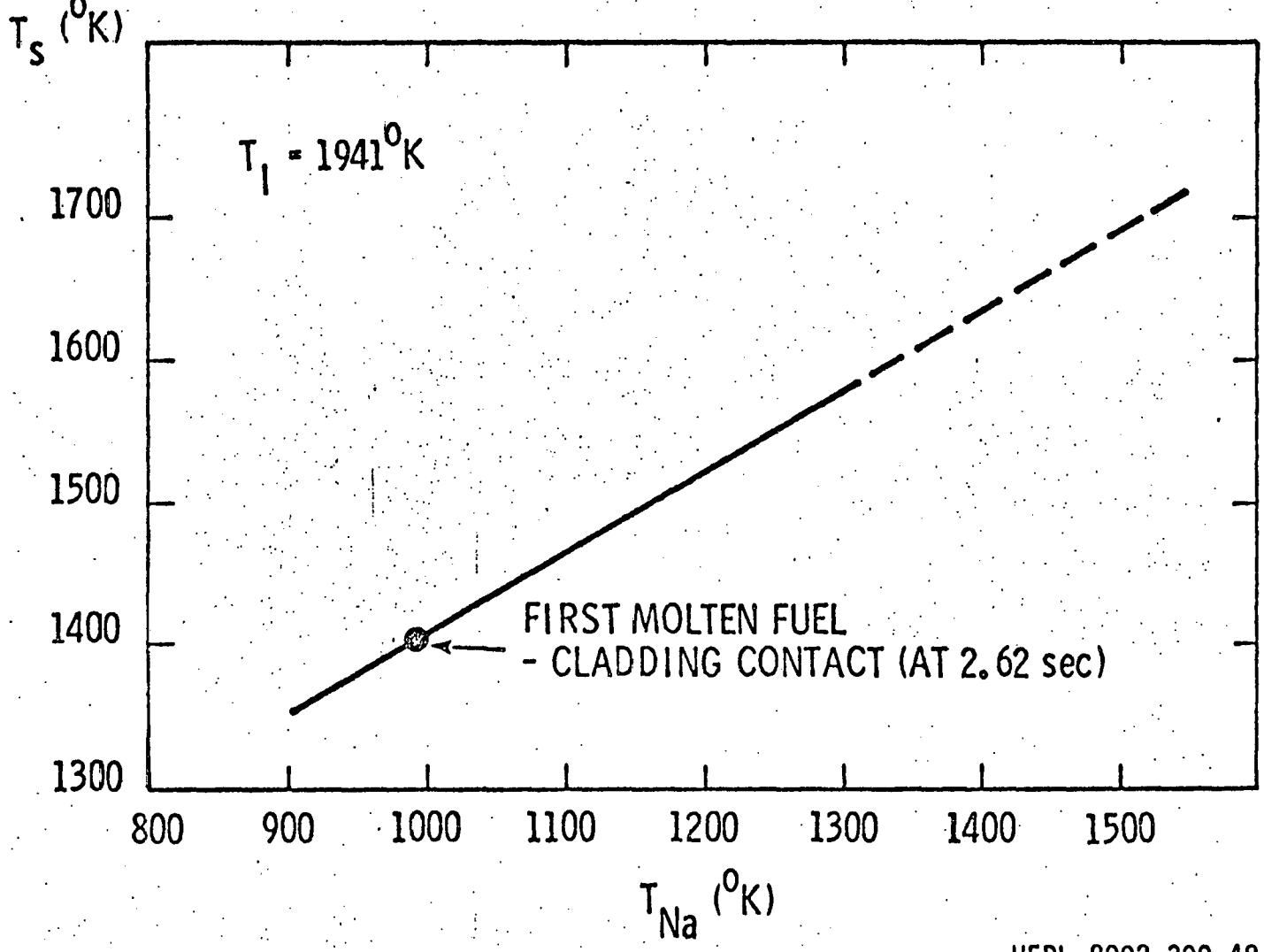

FIGURE 18. Variation of Cladding Outer Surface Temperature with Sodium Temperature (T_I = 1941°K).

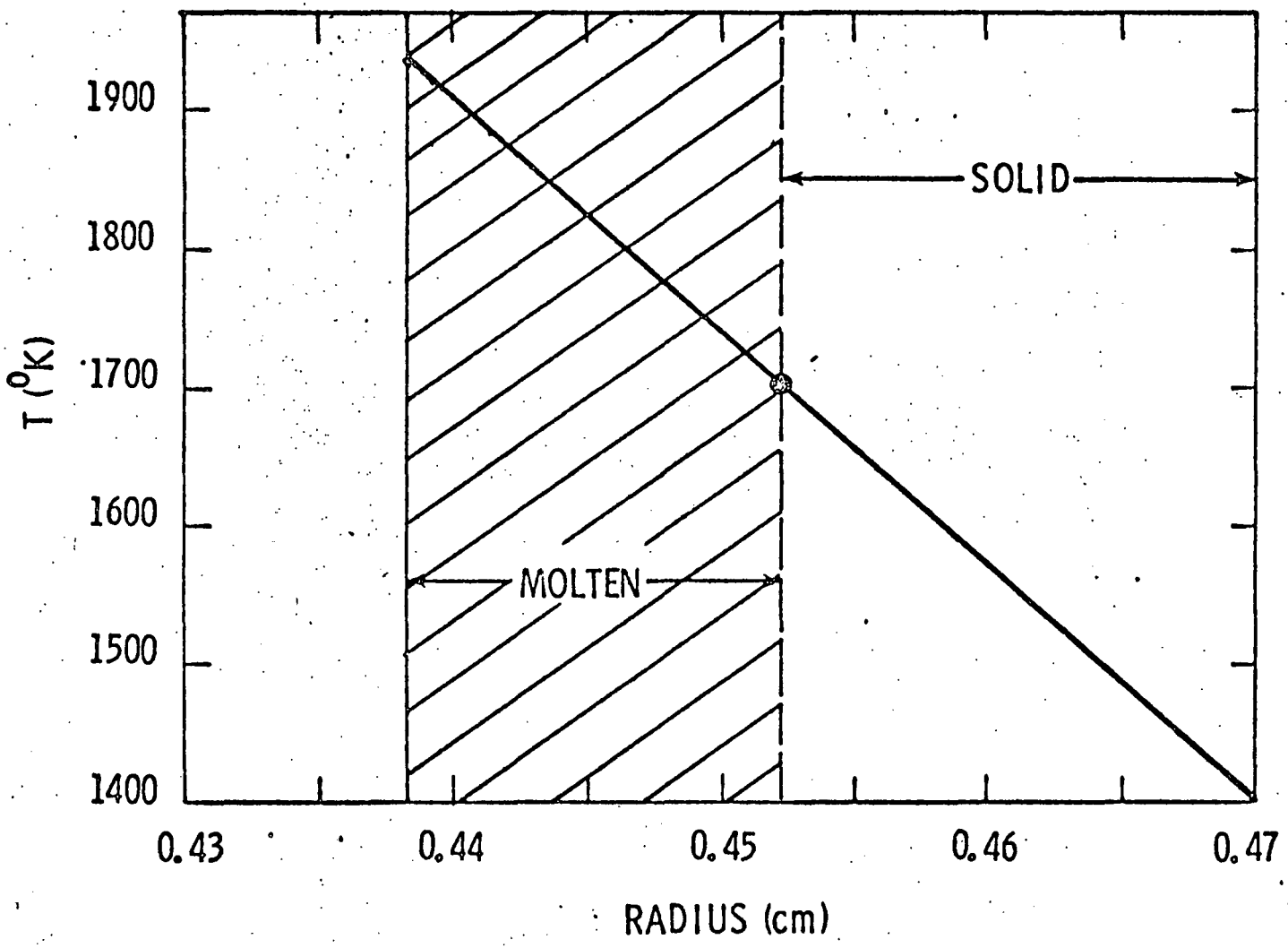

FIGURE 19. Radial Cladding Temperature on Contact With Molten Fuel. HEDL 8002-300.49

THIS PAGE

WAS INTENTIONALLY

LEFT BLANK

failure would have certainly taken place if the gap were closed. However, an open gap introduced some uncertainty in the prediction of cladding failure at this time.

The calculations in Section (a) indicated cyclic variations in cladding temperature, caused by molten fuel which cooled on contact with cladding. These temperature variations would have weakened the cladding. To be conservative, a delayed time of failure was considered, at 2.80 sec into the transient (a later time of failure produced a larger molten fuel fraction and a higher fuel temperature). At this time, about 20% of fuel had melted, condition (2) on the differential volume thermal expansion was well satisfied, and the fuel had long reached its break-up internal pressure. Bond boiling had proceeded up and down the upper 2/3 of the fuel. The location of failure was taken at MELT node 18 (core node 12), where surface fuel melting first occurred and the cladding had weakened most from long cyclic temperature variations. In fact, by the same token, cladding could fail anywhere along the upper third of the pin, but a lower location at node 18 was assumed, again for conservatism, to give worse sodium voiding and fuel motion reactivity feedbacks.

IV. SUMMARY AND CONCLUSIONS

For the He-bonded carbide elements (channel #8) the location of cladding failure was determined to be at MELT core node 11, about 10 cm above core midplane. Cladding failed at 1.91 sec, but molten fuel-coolant contact was deferred until 2.40 sec into the transient. There was indication that this might occur earlier, but the later time of 2.40 sec was thought to be conservative, in that more molten fuel was present at the time of first fuel ejection. In fact, at this time there was only 17.5 gm of molten fuel in the carbide pin compared to 65 gm at the time of first fuel ejection in the oxide channel #2.

To date, the only TREAT test of a He-bonded carbide pin up to cladding breaching was the HC3 test. The test simulated a $.50/sec ramp in the FTR. Comparison is complicated by the difference in pin dimensions and irradiation conditions (Table 1) as well as possible difference in transient conditions (Table 2). Early post-irradiation examination (PIE) indicated no fuel melting. More recent PIE found evidence of fuel melting around the area of breached cladding. However, it was not known whether fuel melting occurred prior to or after cladding failure. The pin peak power in the test was 75.9 kW/ft (249 kW/m). At the time of cladding failure in channel #8, UNCLE-T calculated a pin peak power of 94 kW/ft. Thus, based on pin peak power, cladding failure in the HC3 test occurred even earlier than the He-bonded pin considered in this study. However, the HC3 pin had a much higher burnup (6.2 a/o versus 2.89 a/0). There was no information on the time and location of failures in the HC3 test.

The prediction of pin failure for the Na-bonded pin (channel #9) was more uncertain. Due to the large fission gas retention prior to the transient, this pin reached the assumed break-up internal pressure at 2.62 sec, much sooner following fuel melting than the He-bonded pin (40 msec versus 300 msec). At this time, the fuel melt fraction was still very small (0.73%). The fuel-cladding gap which remained open kept the cumulative damage fraction low, and cladding failure was not certain. However, it appeared difficult to argue against pin failure at 2.80 sec into the transient, when about 20% of fuel had melted and about 50% of fuel surface attained solidus temperature, mainly along the upper half of the fuel pin. The failure location was likely to be at cladding hot spots, at or above a distance 2/3 from fuel bottom. Along this upper third of the element, LOB by boiling had began about 900 msec earlier causing molten fuel to slump on cladding shortly later. Slumping fuel cooled on contact with cladding causing a cyclic variation in cladding temperature with an upward trend, reducing thereby cladding strength.

TABLE 1

COMPARISON BETWEEN SOME TREAT TESTS AND CARBIDE FUEL IN THIS STUDY

	C #8	HC3	C #9	SC1-A	SC3
Pellet Density (%TD)	81	87		98	98
Bond Type	Helium	Helium	Sodium	Sodium	Sodium
Diametrical Gap (cm)	0.015	0.025	0.091	0.081	0.081
Fuel-Column Length (cm)	91.4	34.3	91.4	34.3	34.3
Cladding Material	316 SS, 20% cw	316 SS, 20% cw	316 SS, 20% cw	316 SS, 20% cw	316 SS, 20% cw
Cladding OD (cm)	0.94	0.787	0.94	0.787	0.787
Cladding Thickness (cm)	0.051	0.051	0.038	0.038	0.038
Burnup (at%)	2.712 (max)	6.1	2.712 (max)	0	8.4
Steady-State Power (kW/ft)	22.75	22.86	22.75		22.86

TABLE 2

SUMMARY OF TREAT TESTS ON CARBIDE FUEL ELEMENTS*

	HC1	SC1	SC1-A	HC2	SC3	HC3	SC4
Purpose	Calibration	Integrity Margin Demonstration	Bond Behavior Investigation	Integrity Margin Demonstration	Integrity Margin Demonstration	Breaching Threshold Determination	Breaching Threshold Comparison (via HC3)
Fuel Element	K6B	AIR-1 (shrouded)	AIR-1 (shrouded)	K6B-86	AIR-1-100	K6B-84	K7-6
Pellet Density/Gap Size (mils)	87/10	98/26	98/26	87/10	98/26	87/10	98/26
Burnup (a/o)	0	0	0	6.3	8.4	6.2	8.3
Thermally Simulated FTR Ramp	60¢/s	80¢/s	70¢/s	50¢/s	50¢/s	50¢/s	50¢/s
Peak Pin Power in TREAT (kW/m)	120	250	384	164	148	249	245
Simulated FTR Pin Power (kW/m)	120	250	384	233	250	420	400
Nuclear Energy Deposition (J/g)	770	1100	1850	1080	1150	1830	1640
Peak Fuel Temp. (°C)	1650	1600	2480	1600	1350	2300	1850
Peak Midwall Clad Temp. (°C)	650	870	990	720	700	970	980
Cladding Integrity	Maintained	Maintained	Maintained	Maintained	Maintained	Breached	Maintained
Cladding Damage	No	No	Ovality, Incipient Cracks	D/D = 0.1%	No	Longitudinal Cracks	D/D = 0.36%
Fuel Damage	Mild Cracking	No	Estensive Cracking, Separation	No	No	Cracking and Swelling	Minimal
Bond Damage	--	No	Bond Boiling	--	Minor	--	Poor bond quality before test--bond disturbances indicated during test

*Taken from Ref. 7

Again, experimental data for a definitive comparison with calculations are lacking. The SC1-A post-test examination indicated that the Na-bond voided from boiling, but that no fuel melting occurred. Cladding integrity was preserved, indicating that the bond vapor did not produce a pressure sufficient to burst cladding. These results agree with the present calculations. It is believed that this comparison of bond behavior remains valid, in spite of the fact that the SC1-A test used an unirradiated pin.

A significant result from the SC1-A test is the recent discovery that LOB by boiling did not occur instantaneously. Test data suggest that incipient sodium-bond boiling occurred at a superheat of 110°C and that bond boiling lasted for 0.8 sec before complete bond voiding. The impact of this phenomenon would be to delay fuel melting and pin failure, but not necessarily to increase fuel temperature at failure. The resulting change in the HCDA consequences would be minimal.

V. REFERENCES

1. A. E. Waltar, et al., An Analysis of the Unprotected Transient Overpower Accident for the FFTF, HEDL-TME 75-50, Hanford Engineering Development Laboratory, Richland, WA, June 1975.

2. M. C. Billone, et al., "Analysis of Carbide and Nitride Fuel-Element Performance Using UNCLE-T," Trans. Am. Nucl. Soc., 24, 135 (1976)

3. A. E. Waltar, et al., MELT-III: A Neutronics, Thermal-Hydraulics Computer Program for Fast Reactor Safety Analysis, HEDL-TME 74-47, Hanford Engineering Development Laboratory, Richland, WA, December 1974.

4. D. S. Dutt and R. B. Baker, SIEX - A Correlated Code for the Prediction of Liquid Metal Fast Breeder Reactor Fuel Thermal Performance, HEDL-TME 74-55, September 1974.

5. Letter from A. L. Schwallie (W-ARD), to N. DeMuth (LASL), January 16, 1979, "ACN-1 Revised Coolant and Cladding Temperatures and Uncertainty Factors."

6. K. Q. Baley, et al., "UK Irradiation Experience Relevant to Advanced Carbide Fuel Concepts for LMFBR's," Proc. of the Int. Meeting on Advanced LMFBR Fuels, Tucson, AZ, October 10-13, 1977.

7. "Advanced Fuels Development Program - Quarterly Progress Report, April-June 1979," ANL-AFP-73, Argonne National Laboratory, Argonne, IL.

8. M. C. Billone, et al., "Progress in Modeling Carbide and Nitride Fuel Performance in Advanced LMFBRS," Proc. of the Int. Meeting on Advanced LMFBR Fuels, Tucson, AZ, October 10-13, 1977.

9. H. C. Tsai, et al., "Behavior of Advanced Carbide Fuel During Transient Overpower Operations," Proc. of the Int. Conference on FBR Fuel Performance, Monterey, CA, March 5-8, 1979.

10. H. C. Tsai and L. A. Neimark, "Cladding Damage Analysis Applied to Carbide TREAT Tests HC2 and HC3, Trans. Am. Nucl. Soc., 32, 223, June 1979.

11. "Advanced Fuels Development Program - Monthly Status Letter, December 1979," ANL-AFP-80, Argonne National Laboratory, Argonne, IL.

12. G. D. Johnson and C. W. Hunter, Mechanical Behavior of Fast Reactor Fuel Pin Cladding Subjected to Simulated Overpower Transients, HEDL-TME 78-13, Hanford Engineering Development Laboratory, Richland, WA, June 1978.

13. Joanne K. Fink, et al., Thermal Physical Properties of Thorium and Uranium Systems for Use in Reactor Safety Analysis, ANL-CEN-RSD-77-1, Argonne National Laboratory, Argonne, IL, June 1977.

14. A. Sheth and L. Leibowitz, Equation of State and Transport Properties of Uranium and Plutonium Carbides in the Liquid Region, ANL-AFP-11, Argonne National Laboratory, Argonne, IL, September 1975.

15. J. P. Holman, Heat Transfer, 3rd Edition, McGraw-Hill Book Company, p. 40, 1972.

16. Glen E. Myers, Analytical Methods in Conduction Heat Transfer, McGraw-Hill Book Company, pp. 201-202, 1971.